THE JOURNAL OF PHYSICAL CHEMISTRY B

Article

pubs.acs.org/JPCB

Temperature-Dependent Hole Mobility and Its Limit in Crystal-Phase P3HT Calculated from First Principles

Andreas Lücke,[†] Frank Ortmann,[‡] Michel Panhans,[‡] Simone Sanna,[†] Eva Rauls,[†] Uwe Gerstmann,[†] and Wolf Gero Schmidt*[,†]

[†]Lehrstuhl für Theoretische Materialphysik, Universität Paderborn, 33095 Paderborn, Germany

[‡]Institute for Materials Science and Dresden Center for Computational Materials Science, Technische Universität Dresden, 01069 Dresden, Germany

ABSTRACT: We study temperature-dependent hole transport in ideal crystal-phase poly(3-hexylthiophene) (P3HT) with ab initio calculations, with the aim of estimating the maximum mobility in the limit of perfect order. To this end, the molecular transfer integrals, phonon frequencies, and electron−phonon coupling constants are obtained from density functional theory (DFT). This allows the determination of transport properties without fit parameters. The strong coupling between charge carriers and vibrations leads to strong scattering and polaronic effects that impact carrier transport. By providing an intrinsic mobility limit to ideal P3HT crystals, this work allows identification of the impact of disorder on the temperature-dependent transport in real samples. A detailed analysis of the transport-relevant phonon modes is provided that gives microscopic insight into the polaron effects and hints toward mobility optimization strategies.

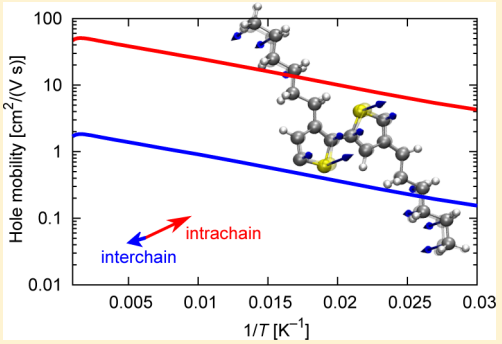

1. INTRODUCTION

Poly(3-hexylthiophene) (P3HT) is one of the most studied organic semiconductors with *p*-type transport characteristics, which, however, exhibits only moderate carrier mobility. To estimate the possible limit of hole conduction in this polymer, it is helpful to understand the underlying charge-transport processes and the impact of vibrations in detail. In addition, a detailed knowledge on the impact of disorder and how to reach this limit is desirable. In fact, numerous publications address the conductivity of P3HT: Improved transport properties have been reported for chains with high molecular weight (MW) in refs 1−4 and have been associated with band transport in films composed of long polymer chains[5] whereas hopping processes dominate in low-MW polymer films. The conductivity of high-MW polycrystalline P3HT films was found to be highly anisotropic, with smaller mobilities being perpendicular to the chains rather than parallel to them.[6−8] In addition, the influence of temperature,[2,4,9−13] frequency,[14,15] electric field,[2,16,17] structure,[2,11,13−15,17−23] external strain,[24−26] and oxidation[27−33] on the transport properties of P3HT was investigated experimentally and theoretically.

Many molecular dynamics studies have been performed to analyze the influence of temperature on the P3HT structure and transfer integrals (see, e.g., refs 11, 13, 18, and 23). Frequently, temperature-dependent experimental conductivities have been fitted with analytical expressions to understand the findings in terms of models based on an effective vibration and the associated phonon frequency and electron−phonon coupling constant (see refs 2, 34, and 35). Moreover, disorder effects were accounted for using mobility-edge models that separate the density of states into immobile (trapped) and mobile states to reproduce experimental data[36−38] with fitted parameters. These approaches can, therefore, give first indications on the maximum intrinsic carrier mobilities when traps are reduced. However, theoretical models that rely on fit parameters obtained from experimental data have difficulty in separating the respective influence of disorder and intrinsic polaronic effects on the mobility.[39]

This theoretical work focuses on the *first-principles* description of idealized P3HT crystals and is based on the Kubo formalism[40] and a Holstein Hamiltonian,[41] for which the material parameters, including all optical phonon frequencies and electron−phonon coupling constants, are obtained from density functional theory (DFT). This enables us to describe the transport properties of P3HT, including polaron effects. Charge carrier localization at defects and the related hopping phenomena are not considered. Thus, this study provides an upper mobility limit by considering transport in a perfectly ordered structure. We also analyze the impact of specific vibrational modes and the variability of transport by tuning these modes.

2. METHODOLOGY

2.1. Charge-Transport Theory. Recently, a transport theory for organic crystals based on the Kubo formula and the Holstein Hamiltonian has been developed.[42] The electron−

Received: April 8, 2016
Revised: May 27, 2016
Published: June 1, 2016

DOI: 10.1021/acs.jpcb.6b03598
J. Phys. Chem. B 2016, 120, 5572−5580

phonon interaction is described using electron−phonon coupling constants (g_λ) for the individual phonon modes (λ). For the evaluation of mobility, we integrate local and nonlocal couplings that are present in P3HT in a set of effective coupling constants according to $g_\lambda^2 = \sum_i g_{\lambda i}^2$ for each mode (λ). The total charge carrier mobility in this theoretical framework includes phonon-assisted contributions[42]

$$\mu_{\alpha\beta}^{(\mathrm{I})} = -\frac{1}{e_0 N_c 2k_B T}\left(\frac{e_0}{\hbar}\right)^2 \sum_{LMN} \mathbf{R}_{L\alpha}\tilde{\epsilon}_L \mathbf{R}_{N\beta}\tilde{\epsilon}_N \times \frac{1}{N_\Omega}\sum_{\mathbf{k}_1\mathbf{k}_2} e^{-i\mathbf{k}_1(\mathbf{R}_M+\mathbf{R}_N)} e^{i\mathbf{k}_2(\mathbf{R}_M-\mathbf{R}_L)} n_{\mathbf{k}_1}(1-n_{\mathbf{k}_2}) \times \int_{-\infty}^{\infty} dt\; e^{(it/\hbar)[\tilde{\epsilon}(\mathbf{k}_1)-\tilde{\epsilon}(\mathbf{k}_2)]} \times \{\exp[-(\delta_0^M - \delta_L^M - \delta_{-N}^M + \delta_{L-N}^M) \times \sum_\lambda (N_\lambda e^{i\omega_\lambda t} + (1+N_\lambda)e^{-i\omega_\lambda t})g_\lambda^2] - 1\} e^{-(t/\tau)^2} \quad (1)$$

which are dominated by purely incoherent terms at higher temperatures, such as in the Marcus theory and in variable-range hopping approaches. The indices L, M, and N in eq 1 run over the next-nearest neighbors (lattice vector $\mathbf{R}$) in the **a** and **c** directions (the transfer integral in the **b** direction is negligible; see below), and the $\mathbf{k}$ sum runs over the first Brillouin zone. $n_\mathbf{k}$ is the Fermi occupation for the state with energy $\tilde{\epsilon}_\mathbf{k}$. Furthermore, $N_c/N_\Omega = 10^{-6}$ is the charge carrier concentration per unit cell and $\hbar/\tau = 0.1$ meV is a small parameter that is chosen for consistency with the limit of ultrapure crystals. The total mobility calculated for the temperature range considered here is numerically robust with respect to τ: It changes only by a few percent at low temperatures (<100 K) if τ is doubled or halved (remaining in the ultrapure limit). Beyond being just a numerical parameter in the first place, τ can also be assigned an additional role as the effective scattering time. This is given in the Appendix.

Assuming complete phonon dressing of the charges, the polaron transfer integrals $\tilde{\epsilon}$ are determined from the electron transfer integrals ϵ of the crystal as

$$\tilde{\epsilon}_M = \epsilon_M \exp[-\sum_\lambda (1+2N_\lambda)g_\lambda^2] \quad (2)$$

where N_λ denotes the Bose−Einstein distribution function for the phonon mode with energy ω_λ.

The second contribution to the mobility stems from the coherent band transport according to

$$\mu_{\alpha\beta}^{(\mathrm{II})} = \frac{\sqrt{\pi}e_0\tau}{2N_c\hbar^2 k_B T}\sum_{\mathbf{k}_1} n_{\mathbf{k}_1}(1-n_{\mathbf{k}_1})\frac{\partial\tilde{\epsilon}(\mathbf{k}_1)}{\partial k_\alpha}\frac{\partial\tilde{\epsilon}(\mathbf{k}_1)}{\partial k_\beta} \quad (3)$$

The sum of both parts yields the total mobility and is studied throughout the article. This method has already been proven successful for studying the transport properties of naphthalene,[43,44] durene,[44,45] and guanine[44,46] in the relevant temperature regime.

2.2. Ab Initio Simulations. To evaluate the above formulas for P3HT, its electronic and vibrational properties have to be determined. For that, we use DFT, as implemented in the Vienna ab initio simulation package.[47] Bulk P3HT is modeled using a supercell with periodic boundary conditions. Projected augmented wave pseudopotentials[48] are used to describe the ion−electron interaction. The generalized gradient approximation is used with the Perdew−Burke−Ernzerhof functional[49,50] to describe the electronic many-body interactions. Dispersion interaction is known to influence the structural properties of soft matter such as P3HT aggregates.[51] Here, dispersion is taken into account using the so-called DFT-D approach, that is, a semiempirical London-type correction term[52−54] with the parameters suggested by Grimme[55] (DFT-D2).

Plane waves up to an energy cutoff of 400 eV are used as the basis set for the expansion of electron wave functions. Monkhorst−Pack meshes of special $\mathbf{k}$ points[56] are used to sample the Brillouin zone. Specifically, we use 16 $\mathbf{k}$ points in the interchain direction (**a**), 8 in the intrachain direction (**c**), and 4 along the hexyl-side-chain direction (**b**) (cf. Figure 1).

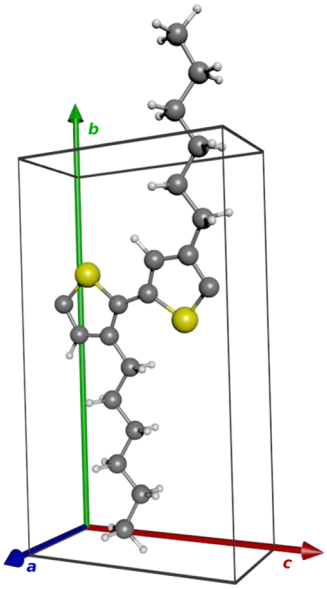

Figure 1. P3HT monomer with its unit cell. Large, medium, and small balls indicate S, C, and H atoms, respectively.

The P3HT crystal is modeled based on a HT-P3HT monomer consisting of 50 atoms within a unit cell, as described in ref 51 (cf. Figure 1), and with periodic boundary conditions applied. From DFT calculations, we obtain 150 phonon frequencies and displacement patterns as well as the electronic band structure of P3HT. The uppermost valence band corresponding to the molecular highest occupied molecular orbital (HOMO) is fitted to a tight-binding model

$$\epsilon(\mathbf{k}) = \epsilon_0 + 2\epsilon_a\cos(\mathbf{k}\cdot\mathbf{a}) + 2\epsilon_c\cos(\mathbf{k}\cdot\mathbf{c}) + 2\epsilon_{2c}\cos(2\mathbf{k}\cdot\mathbf{c}) + 2\epsilon_{3c}\cos(3\mathbf{k}\cdot\mathbf{c}) \quad (4)$$

where ϵ_0 is an energy offset that does not influence the result. The electron−phonon coupling constants $g_{\lambda i}$ for all phonons λ and all directions ($i = 0$ for local coupling and i = **a**, **c**, **2c**, **3c** for nonlocal coupling) are obtained by numerical differentiation of the transfer integrals to the phonon displacement (see ref 59 for details) and enter the calculation of the effective coupling constant g_λ for each individual mode.

3. RESULTS

3.1. Material Parameters. The set of transfer integrals is obtained as $\epsilon_a = 162$ meV, $\epsilon_c = 421$ meV, $\epsilon_{2c} = -26$ meV, and $\epsilon_{3c} = 22$ meV. We note that the band structure (eq 4) does not

DOI: 10.1021/acs.jpcb.6b03598
J. Phys. Chem. B 2016, 120, 5572−5580

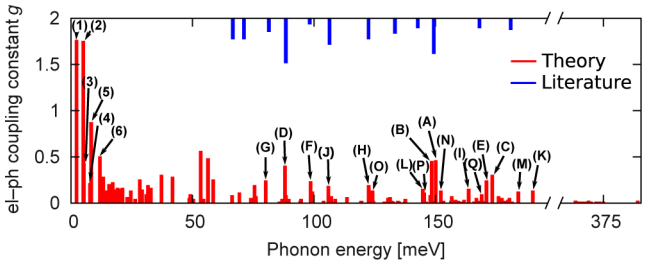

Figure 2. Electron–phonon coupling constants for P3HT. The present calculations (red) are compared with a set of experimentally determined modes from refs 57 and 58 (blue, redshifted by 4 meV). Note that the references provide relative coupling strengths only. The labeled phonon modes are visualized in Figures 5 and 6. We observe a phonon gap between 190 and 363 meV, which has been suppressed in the figure.

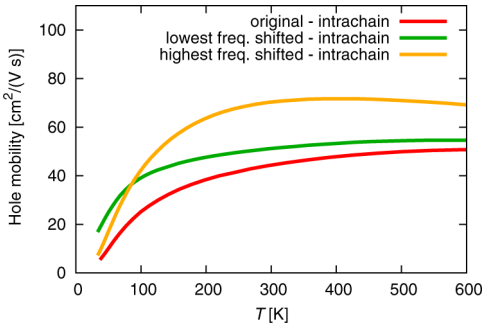

Figure 4. Calculated hole mobility assuming that the six lowest phonon frequencies are increased by 10% (green) or that the phonon frequencies larger than 80 meV are increased by 10% (orange) in comparison with the actual values (red).

contain a transfer integral in the hexyl-side-chain direction (**b**), as it turned out to be negligible.

The calculated electron–phonon coupling constants are summarized in Figure 2 and are compared with those given in available literature data. We find that the vibrational spectrum is dominated by strongly coupling modes at low energies (indicated as modes **1**–**6** in Figure 2). Their large coupling strengths are a consequence of their low frequencies, which enter inversely as a prefactor in the coupling constant calculation.[59] Additional relevant phonon modes are labeled in Figure 2 and are discussed in detail below. Unfortunately, there are no literature data available for phonon frequencies below 70 meV. However, for the data available, the phonon frequencies and coupling strengths calculated here agree well[60] with the parameters determined in refs 57 and 58.

3.2. Hole Mobilities. On the basis of the above material parameters, we calculate the hole mobility in P3HT from eqs 3 and 1. The results are shown in Figure 3a,b as linear and Arrhenius plots, respectively. Mobilities reach about 50 $cm^2/(V\ s)$ and increase with temperature. At high T, this increase starts to saturate. Such large intrinsic mobilities in ideal P3HT crystals are conveyed by large electronic coupling along the polymer chain with dominating ε_c = 421 meV. Despite this large transfer integral, the dominating mobility contribution results from phonon-assisted transport (eq 1), which is largely due to the strong coupling modes with low vibrational energies. As shown in Figure 2, many strong coupling modes occur that suppress the coherent transport but still produce high phonon-assisted mobilities with an activation behavior as discussed below.

While comparing the present calculations with measurements, it should be kept in mind (1) that experimentally an average mobility is measured that also accounts for charge carriers that are trapped[39,61,62] and (2) that the present calculations are performed for a perfect P3HT crystal. Thus, the calculated mobilities represent a limiting case for idealized conditions. Therefore, we compare our results with the experiment-based estimates of intrinsic mobilities. Because of the experimental challenge for P3HT to enter the regime of non-trap-limited mobilities,[5,39,63–65] several authors have attempted to obtain such indirect estimates of intrinsic mobilities. One approach amounts to fitting the temperature-dependent transport data to a mobility-edge model. This estimate yields effective mobility values of about 1 $cm^2/(V\ s)$[37,61] (with some variability), which are orders of magnitude larger than the range of trap-limited values typically encountered.[5,39,63–65] The present calculations based on a disorder-free model result in higher intrinsic values than the estimates obtained in the mobility-edge model from the trap-limited transport but agree well with the theoretical work of Northrup.[66] He calculated a mobility of 31 $cm^2/(V\ s)$ at room temperature employing an acoustic deformation potential scattering model.[67]

We extract an activation energy for transport of about 8 meV from the Arrhenius dependence over a large temperature range shown in Figure 3b. As expected, this energy value is lower than that in trap-limited transport regimes and is consistent with the high mobilities calculated here.

Experimental activation energies were found to depend strongly on the presence of defects, such as grain boundaries,[68–70] and values between 50 and 140 meV[39,71] are

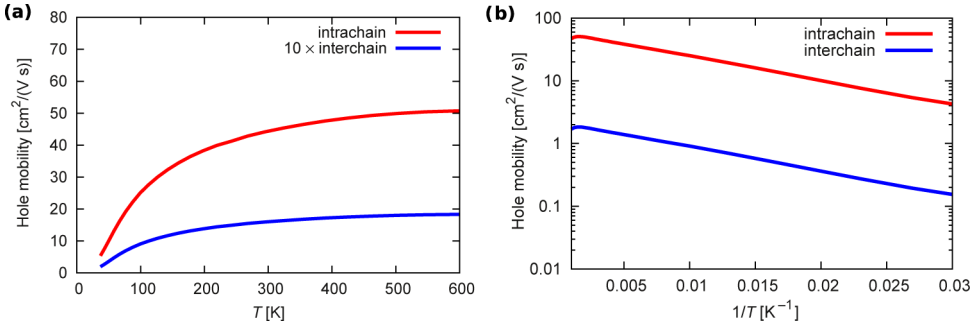

Figure 3. (a) Transport results for a P3HT crystal in the intrachain and interchain directions. The coherent transport contribution is negligible in the depicted temperature range. (b) Same data as in (a) but as an Arrhenius plot.

DOI: 10.1021/acs.jpcb.6b03598
J. Phys. Chem. B 2016, 120, 5572–5580

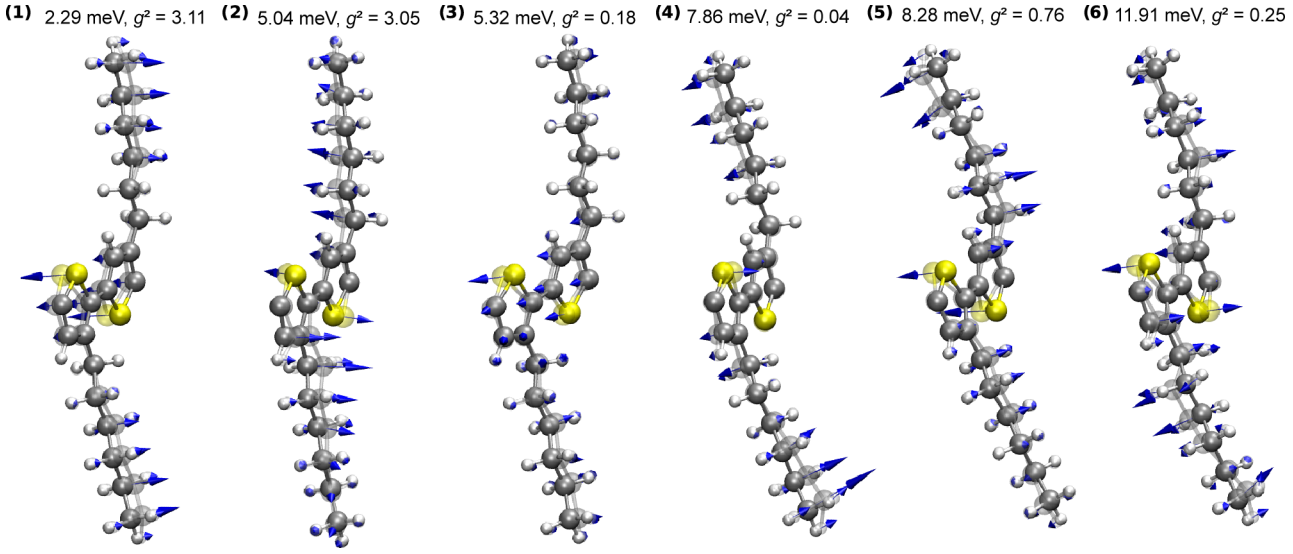

Figure 5. Calculated eigenvectors of the relevant soft phonon modes (see text). The indicated energies are phonon energies $\hbar\omega$ in meV.

reported. Even in high-MW films, the P3HT chains are strongly kinked and folded,[65,71] which will increase the activation energy distinctly above its intrinsic value. By factorizing the effective mobility as the product of a disorder and a polaron term, Chang et al. determined activation energies between 5 and 30 meV.[39]

Figure 3 shows the calculated transport anisotropy for interchain and intrachain mobilities, which reaches a factor of about 25. The interchain transport shows a similar temperature activation as the intrachain transport. Experimentally, the intrachain mobility is at least an order of magnitude larger than the interchain mobility,[70] similar to the present calculations. The mobility anisotropy decreases clearly, however, with increasing temperature because of melting effects.[72] Melting as well as thermally induced crystallization and creation of small crystallites with additional grain boundaries and a reduced number of bridging chains[73] is not included in the present theory.

We note that in our approach the polaron dressing related to very soft phonon modes might also be modeled as a static disorder because of their low vibration frequencies. To explore the robustness of our maximum mobility values with respect to such a modified treatment, we performed additional calculations where the soft phonon modes are modeled as effective temperature-dependent disorders; see Appendix A.1 for details. The mobilities resulting from this approach are somewhat larger (increased by at most a factor of 2 for the studied temperatures) but essentially confirm the order of magnitude for the hole mobilities presented in Figure 3.

Here, we focus on the general impact of the low-frequency vibrations on the carrier mobility, which is analyzed in more detail in the next section.

3.3. Influence and Tuning of Molecular Vibrations. To obtain a deeper understanding of how phonons modify the intrinsic charge transport and to possibly assist molecular design in this regard, the influence of the most relevant phonon modes on the transport characteristics is studied in detail. For this purpose, the phonon frequencies are varied. This implies variations of the electron−phonon coupling constants according to $g_\lambda \sim \omega_\lambda^{-3/2}$. We compare two different scenarios that analyze the possibility of increasing the mobility by reducing the electron−phonon couplings through increased mode frequencies (by 10%). Low- and high-energy modes are considered separately in the two cases: (1) modification of high-frequency modes (modes with energies above 80 meV) and (2) modification of low-frequency modes (lowest six modes; see Figure 5). For instance, the latter scenario could be realized by making the P3HT polymer backbone less flexible.

The resulting temperature-dependent mobilities are plotted in Figure 4. We observe that a frequency blueshift by 10% for the lowest six phonon modes increases the low-temperature mobility considerably but has less influence on temperatures at or above room temperature (8−15% increase). Thus, stiffening the polymer matrix to lock the torsional modes (or at least increase their vibrational frequency) can indeed moderately improve the transport properties of P3HT.

In the second scenario, transport calculations are performed with blueshifted high-energy modes. Their importance for transport in a variety of molecular systems is well known.[74] We increase the frequency of modes above 80 meV by 10% (compare with Figure 6 for strong coupling modes). As a result, the hole mobilities are increased considerably, in particular at room temperature and above (orange line in Figure 4). An increase in the mobility is expected in both scenarios based on the argument of decreasing polaron binding energy $E_{\mathrm{pol}} = \sum_\lambda (1/2) g_\lambda^2 \hbar\omega_\lambda$. This energy acts as a barrier for the phonon-assisted transport. The larger increase in mobility upon tuning the high-frequency modes is due to their stronger contribution to E_{pol}.

As can be seen in Figure 4, the increase in mobility by tuned low-frequency modes is larger than that by the high-frequency modes only at low temperatures. To understand this effect, we evaluate eq 1 analytically, assuming that there are only two effective phonon modes—one with a low frequency ($\hbar\omega_1 < k_B T$) and the other with a high frequency ($\hbar\omega_2 > k_B T$). The mobility depends on the frequencies and coupling constants (g_1 and g_2) according to (see Appendix A.2 for a derivation)

DOI: 10.1021/acs.jpcb.6b03598
J. Phys. Chem. B 2016, 120, 5572−5580

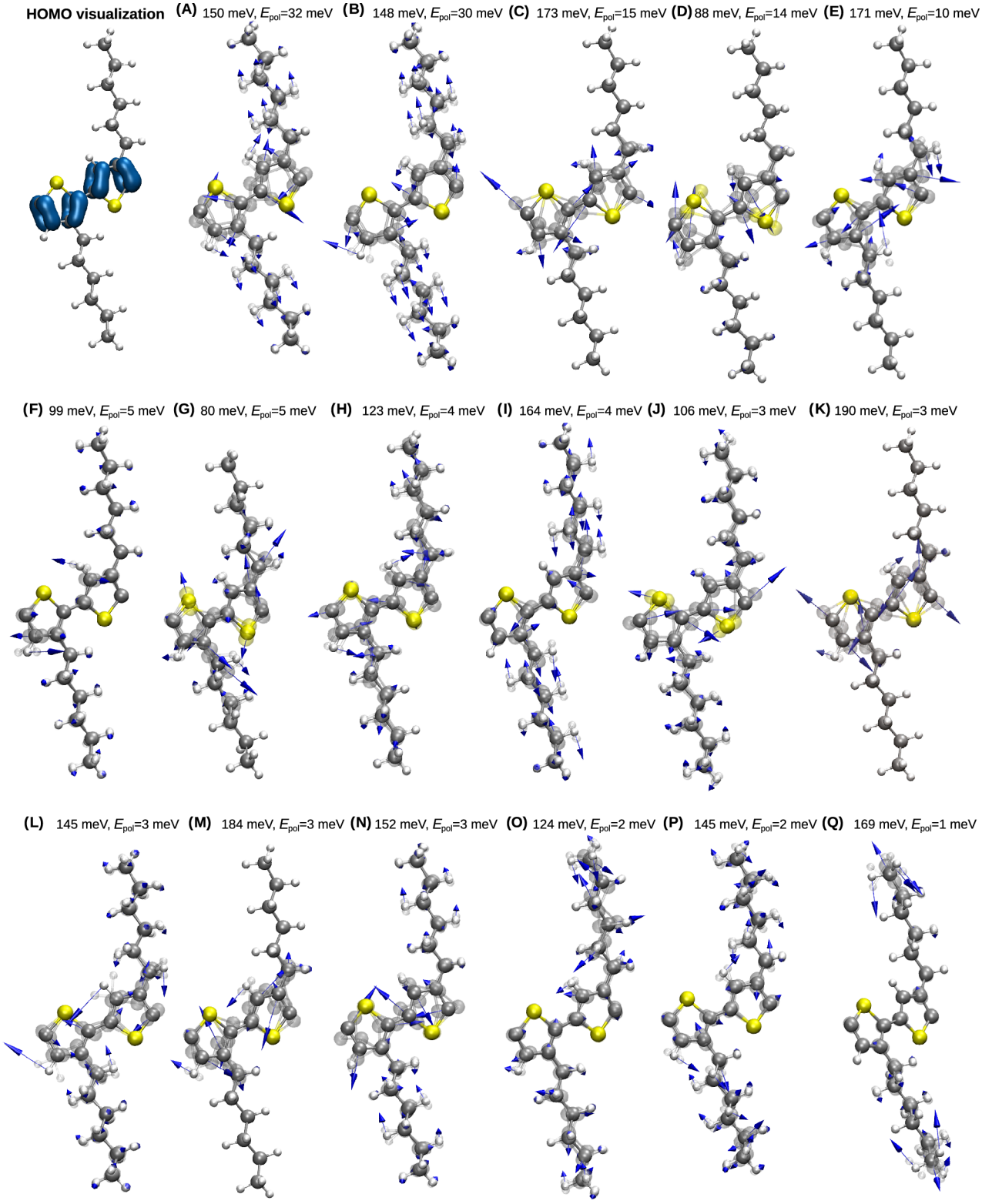

Figure 6. Calculated eigenvectors of relevant high-energy phonon modes above 80 meV, ordered according to their polaron binding energy. The indicated energies are phonon energies $\hbar\omega$ in meV. The HOMO orbital character is indicated on top left.

$$\mu \sim \frac{1}{\omega_1 g_1}\sqrt{\frac{1}{(1+2N_1)}}\, e^{-g_1^2/(1+2N_1)}\cdot e^{-2g_2^2} \approx \sqrt{\frac{\hbar}{g_1^2\omega_1\cdot 2k_B T}}\, e^{-g_1^2\hbar\omega_1/2k_B T}\cdot e^{-2g_2^2} \quad (5)$$

From the above equation, note that the modification of ω_1 to higher values results in a total increase in mobility (because of the reduced coupling $g_1 \sim \omega_1^{-3/2}$), leading to a stronger activation behavior at low temperatures. As the low-frequency modes have much higher coupling constants than the high-frequency modes (cf. Figure 2), their decreased coupling

DOI: 10.1021/acs.jpcb.6b03598
J. Phys. Chem. B 2016, 120, 5572−5580

constants lead to higher mobilities in this low-temperature regime. At higher temperatures, we observe that the increase in mobility is proportional to the increase in the soft mode frequency ω_1. Hence, the absolute mobility improvement due to blueshifted soft modes is as strong as the frequency shift itself (10% in our case).

In contrast, ω_2 has a comparably high energy. This makes its contribution approximately temperature independent ($\sim e^{-2g_2^2}$) but very sensitive to modifications of g_2. Hence, at and above room temperature, the blueshift of the high-frequency modes increases the mobility more strongly. Therefore, it is interesting to identify the important high-frequency phonon modes of P3HT and to investigate their displacement patterns to possibly modify them in P3HT.

The 17 most relevant high-frequency modes are shown in Figure 6, ranked by their contribution to E_{pol}. This ranking differs from a sorting by coupling constants because of a frequency-dependent prefactor. Modes **A** and **B** are most important among the phonons shown in Figure 6. They feature large vibrational amplitudes at the ring carbon atoms and thus strongly affect the HOMO, which explains their relevance to hole mobility.[27] The HOMO, indicated by blue isosurfaces in Figure 6 (top left), corresponds to π states at the C=C ring bonds and has nodes at the inter-ring connection and at the C−C bond opposite to sulfur. Vibrations **D**, **F**, and **M**, which do involve carbon atoms at the thiophene unit but mainly at the node positions of the HOMO, affect the transfer integrals somewhat less. This also holds for modes **K** and **N**, where the stretching and compression of C=C bonds nearly compensate each other because of the asymmetric nature of the vibration. Out-of-plane movements of C atoms (e.g., in mode **J**) are also of little relevance to the transfer integrals, as they are accompanied by small bond length changes only.

Some of the modes discussed above have been identified experimentally: in refs 75 and 76 a strong symmetric C=C mode is reported at 179 meV, in good agreement with the present mode **C**. Furthermore, a weaker antisymmetric C=C mode was detected at 187 meV,[75,76] which is coincident with mode **K** at 190 meV. A C−C stretching mode at 171 meV is also reported in refs 75 and 76, which matches perfectly with mode **E**, where the C−C bonds opposite to the sulfur atom are stretched and compressed. Vibration **G** involving the sulfur atom, which is calculated here at 80 meV, is detected in ref 76 at 84 meV.

High-energy modes involving hydrogen atoms are typically negligible for the relevant transfer integrals. Mode **F** at 99 meV (experimentally detected as "CH out-of-plane bending of the thiophene ring" at 102 meV[76]) is one exception in this respect since it also involves backbone C atoms. Similarly, the influence of the hexyl-side-chain vibrations on the transfer integrals is minor (cf. modes **O**−**Q**) as long as their rotation or stretching and buckling do not affect backbone C atoms as in modes **G**, **H** and **L**.

4. CONCLUSIONS

In summary, *first-principles* calculations for the band structure, phonon modes, and electron−phonon coupling constants together with charge-transport simulations within the Kubo formalism have been performed to predict and rationalize the temperature-dependent hole mobility in ideal P3HT crystals. On the basis of this approach, a well-defined limit for the mobility in a crystalline material is determined, which helps in the interpretation of experimental data in which polaron and disorder effects manifest themselves in qualitatively similar ways.[39] In contrast to soft phonon modes, which exhibit very high electron−phonon couplings, high-frequency molecular vibrations with strong coupling constants are found to reduce hole mobility considerably at room temperature. In particular, modes that deform the C=C bonds in the thiophene rings are detrimental to the charge transport.

Although material modifications that reduce the influence of these modes might moderately improve hole mobility, our calculated mobilities demonstrate that far stronger effects can be expected by further increasing the crystallinity of present P3HT-based devices. A comparison of our theoretical calculations for ideal crystals, including polaron effects, with the measured values of various P3HT films indicates that the experimental samples suffer from significant structural disorder, which influences most strongly the device performance by decreasing the carrier mobility by more than 2 orders of magnitude below its ideal value, which we determine as 50−100 $cm^2/(V\,s)$ at room temperature.

APPENDIX

A.1. Semiclassical Treatment of Soft Modes and Static Disorder

In this section, we consider another variant of our transport approach. For this purpose, the low-frequency modes below a cutoff frequency ($\omega < \omega_C$) are treated semiclassically via the scattering time τ in eqs 3 and 1. In this way, the scattering time can be employed for describing scattering beyond the vibrations that are treated in the polaron framework. A semiclassical treatment of vibrations may be justified when their motion is slow compared with the carrier transport time scale. In such a case, the Holstein (−Peierls) Hamiltonian is restricted to the remaining phonon modes by subtracting the low-frequency contributions $H_{el-pH,low}$. The remaining modes ($\omega > \omega_C$) still contribute to polaron dressing and are treated in the original way as described in Section 2.

A semiclassical treatment of the low-frequency modes induces a change in the potential landscape (because of their electron−phonon coupling) in which the charge carriers move. This potential landscape has to be determined and is obtained from the mean occupation of the modes and their couplings to the onsite energies and transfer integrals. From the knowledge of the variance of the vibrational displacement (the mean is 0) and its impact on the electronic energies according to $\langle H^2_{el-pH,low}\rangle$, we calculate this random disorder potential $H^{static}_{MN} = \sum_\lambda \hbar\omega_\lambda \sqrt{1 + 2\langle N_\lambda\rangle}\, \phi^\lambda_{MN} g^\lambda_{MN}$. Here, we chose ϕ^λ_{MN} at random for all P3HT lattice points M,N (see the corresponding tight-binding model) such that its variance reproduces the temperature-dependent value $\langle H^2_{el-pH,low}\rangle$ caused by all of the modes, λ, with $\omega_\lambda < \omega_C$. We analyze the random disorder potential by fitting a Gaussian to the distribution of onsite energies and transfer integrals and extract their widths σ for each given temperature. Finally, the scattering time $\tau(T)$ is calculated as $\tau = \sqrt{2}\hbar/\sigma(T)$ and is used to evaluate eqs 1 and 3.

We first chose ω_C such that the six lowest phonon modes that couple strongly (see Figure 5) are treated classically, which amounts to setting ω_C = 12 meV. As a result, we observe that the mobility is enhanced at room temperature compared with that in the original treatment (see Figures 3 and A.1). The activation energy calculated within the quasi-static disorder

DOI: 10.1021/acs.jpcb.6b03598
J. Phys. Chem. B 2016, 120, 5572−5580

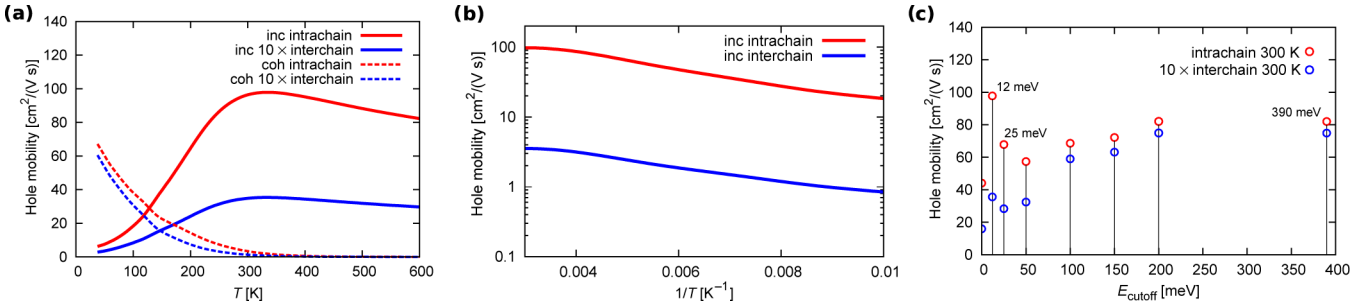

Figure A.1. (a) Transport results for a P3HT crystal in the intrachain and interchain directions where the lowest six phonon modes are not treated quantum-mechanically but as a static disorder. The solid curves depict μ(I) and dashed curves depict coherent transport μ(II). (b) Same data as in (a) but as an Arrhenius plot. (c) Mobility dependence on the cutoff $E_C = \hbar\omega_C$ at 300 K (see text).

model increases to 21 meV. Although the two approaches lead to quantitatively different results, the results are of the same order of magnitude for the calculated hole mobilities at ambient temperatures. The coherent contribution to the mobility is strongly increased compared to that in the original treatment (compare Figures 3 and A.1) and starts to dominate at temperatures below 150 K. We emphasize that such behavior is expected in the absence of traps at the valence band edge, which would strongly reduce the low-temperature mobility. Such a description, however, would require a microscopic modeling beyond the temperature-dependent effective disorder parameter $\tau(T)$, which is outside the scope of this article.

In Figure A.1 we further show the influence of the cutoff frequency (at 300 K) and calculate the total mobility as a function of ω_C. We observe only weak changes for even higher cutoff frequencies up to a classical description of all vibrations at ω_C = 390 meV. Indeed, with the two illustrated cases ($\omega_C = 0$ in Figure 3 and ω_C = 12 meV in Figure A.1), we have already captured the largest and lowest values for room-temperature mobility.

A.2. Two-Phonon Model

To better understand the physics in eq 1 and quantitative changes in the mobilities upon modification of the phonon parameters in Section 3.3, they have been evaluated analytically using several approximations. Because of the large electron−phonon coupling constants in P3HT, the exponential factor in eq 2 leads to a strongly reduced bandwidth for the HOMO, which suggests a narrow band approximation[42] for hole mobility, which can be written as

$$\mu_{\alpha\beta}^{(\mathrm{NBA})} = \frac{e_0(1-c)}{2\hbar^2 k_B T}\sum_L \mathbf{R}_{L\alpha}\mathbf{R}_{L\beta}\epsilon_L^2 I(\omega_1, \omega_2) \tag{6}$$

with

$$I(\omega_1, \omega_2) = \int_{-\infty}^{\infty} \mathrm{d}t \times \exp\{2\sum_\lambda [(1+2N_\lambda)(\cos(\omega_\lambda t) - 1) - \mathrm{i}\sin(\omega_\lambda t)]g_\lambda^2\}\, \mathrm{e}^{-(t/\tau)^2} \tag{7}$$

Furthermore, we apply a two-phonon model with a low-frequency ω_1 and a high-frequency ω_2 such that $\hbar\omega_1 < kT < \hbar\omega_2$. For the high-frequency mode, we approximate its contribution by zero-point vibrations and set $N_2 \approxeq 0$ for the temperature range considered. With these two assumptions, the time integral in eq 7 reads

$$\int_{-\infty}^{\infty} \mathrm{d}t\, \exp[-g_1^2(1+2N_1)\omega_1^2 t^2 - 2\mathrm{i}g_1^2\omega_1 t] \exp[2g_2^2(\mathrm{e}^{-\mathrm{i}\omega_2 t} - 1)] \tag{8}$$

The time integration is solved analytically, and we obtain

$$I(\omega_1, \omega_2) = \hbar\sqrt{\frac{\pi}{2E_{\mathrm{pol},1}\hbar\omega_1(1+2N_1)}}\,\mathrm{e}^{-2g_2^2} \times \sum_{k=0}^{\infty}\frac{(2g_2^2)^k}{k!}\exp\left[-\frac{(\hbar\omega_2\cdot k + 4E_{\mathrm{pol},1})^2}{8E_{\mathrm{pol},1}\hbar\omega_1(1+2N_1)}\right] \tag{9}$$

with the polaron binding energy of the low-frequency mode $E_{\mathrm{pol},1} = (1/2)\hbar\omega_1 g_1^2$.

Only the zeroth order of the k sum is applied in eq 9 as it represents a dominant term in the formula of mobility. Higher orders are suppressed strongly by the high frequency, ω_2, entering the exponential factor. This finally results in the high-temperature limit of the incoherent mobility

$$\mu_{\alpha\beta}^{(\mathrm{NBA})} = \frac{e_0(1-c)}{2\hbar k_B T}\sum_L \mathbf{R}_{L\alpha}\mathbf{R}_{L\beta}\epsilon_L^2 \times \sqrt{\frac{\pi}{4E_{\mathrm{pol},1}k_B T}}\,\mathrm{e}^{-E_{\mathrm{pol},1}/k_B T}\mathrm{e}^{-2g_2^2} \sim T^{-3/2}\mathrm{e}^{-E_{\mathrm{pol}}/k_B T} \tag{10}$$

in accordance with ref 42.

AUTHOR INFORMATION

Corresponding Author

*E-mail: w.g.schmidt@upb.de. Phone: +49 5251 602335.

Notes

The authors declare no competing financial interest.

ACKNOWLEDGMENTS

We are grateful to the Deutsche Forschungsgemeinschaft for financial support (FOR1700, FOR1405, SPP1601, and OR 349/1-1). We thank the Paderborn Center for Parallel Computing (PC²) and the Höchstleistungs-Rechenzentrum Stuttgart (HLRS) and the Zentrum für Informationsdienste und Höchleistungsrechnen Dresden (ZIH) for grants of high-performance computer time. Images 5 and 6 were prepared using VMD[77] and the tachyon renderer.

REFERENCES

(1) Kline, R. J.; McGehee, M. D. Morphology and Charge Transport in Conjugated Polymers. *J. Macromol. Sci., Polym. Rev.* **2006**, *46*, 27−45.

DOI: 10.1021/acs.jpcb.6b03598
J. Phys. Chem. B 2016, 120, 5572−5580

(2) Coropceanu, V.; Cornil, J.; da Silva Filho, D. A.; Olivier, Y.; Silbey, R.; Brédas, J.-L. Charge Transport in Organic Semiconductors. *Chem. Rev.* **2007**, *107*, 926−952.
(3) Nelson, J.; Kwiatkowski, J. J.; Kirkpatrick, J.; Frost, J. M. Modeling Charge Transport in Organic Photovoltaic Materials. *Acc. Chem. Res.* **2009**, *42*, 1768−1778.
(4) Pingel, P.; Zen, A.; Abellón, R. D.; Grozema, F. C.; Siebbeles, L. D.; Neher, D. Temperature-Resolved Local and Macroscopic Charge Carrier Transport in Thin P3HT Layers. *Adv. Funct. Mater.* **2010**, *20*, 2286−2295.
(5) Noriega, R.; Rivnay, J.; Vandewal, K.; Koch, F. P. V.; Stingelin, N.; Smith, P.; Toney, M. F.; Salleo, A. A General Relationship Between Disorder, Aggregation and Charge Transport in Conjugated Polymers. *Nat. Mater.* **2013**, *12*, 1038−1044.
(6) Crossland, E. J. W.; Tremel, K.; Fischer, F.; Rahimi, K.; Reiter, G.; Steiner, U.; Ludwigs, S. Anisotropic Charge Transport in Spherulitic Poly(3-hexylthiophene) Films. *Adv. Mater.* **2012**, *24*, 839−844.
(7) Lan, Y.-K.; Huang, C.-I. A Theoretical Study of the Charge Transfer Behavior of the Highly Regioregular Poly-3-hexylthiophene in the Ordered State. *J. Phys. Chem. B* **2008**, *112*, 14857−14862.
(8) Lan, Y.-K.; Huang, C.-I. Charge Mobility and Transport Behavior in the Ordered and Disordered States of the Regioregular Poly(3-hexylthiophene). *J. Phys. Chem. B* **2009**, *113*, 14555−14564.
(9) Warman, J. M.; de Haas, M. P.; Dicker, G.; Grozema, F. C.; Piris, J.; Debije, M. G. Charge Mobilities in Organic Semiconducting Materials Determined by Pulse-Radiolysis Time-Resolved Microwave Conductivity: π-Bond-Conjugated Polymers versus π-π-Stacked Discotics. *Chem. Mater.* **2004**, *16*, 4600−4609.
(10) Dicker, G.; de Haas, M. P.; Warman, J. M.; de Leeuw, D. M.; Siebbeles, L. D. A. The Disperse Charge-Carrier Kinetics in Regioregular Poly(3-hexylthiophene). *J. Phys. Chem. B* **2004**, *108*, 17818−17824.
(11) Cheung, D. L.; McMahon, D. P.; Troisi, A. Computational Study of the Structure and Charge-Transfer parameters in low-molecular-mass P3HT. *J. Phys. Chem. B* **2009**, *113*, 9393−9401.
(12) Vukmirović, N.; Wang, L.-W. Carrier Hopping in Disordered Semiconducting Polymers: How Accurate is the Miller-Abrahams Model? *Appl. Phys. Lett.* **2010**, *97*, No. 043305, DOI: 10.1063/1.3474618.
(13) Poelking, C.; Andrienko, D. Effect of Polymorphism, Regioregularity and Paracrystallinity on Charge Transport in Poly(3-hexylthiophene) [P3HT] Nanofibers. *Macromolecules* **2013**, *46*, 8941−8956.
(14) Grozema, F. C.; van Duijnen, P. T.; Berlin, Y. A.; Ratner, M. A.; Siebbeles, L. D. A. Intramolecular Charge Transport along Isolated Chains of Conjugated Polymers: Effect of Torsional Disorder and Polymerization Defects. *J. Phys. Chem. B* **2002**, *106*, 7791−7795.
(15) Siebbeles, L. D.; Grozema, F. C.; de Haas, M. P.; Warman, J. M. Effect of Backbone Structure on Charge Transport along Isolated Conjugated Polymer Chains. *Radiat. Phys. Chem.* **2005**, *72*, 85−91.
(16) Rühle, V.; Lukyanov, A.; May, F.; Schrader, M.; Vehoff, T.; Kirkpatrick, J.; Baumeier, B.; Andrienko, D. Microscopic Simulations of Charge Transport in Disordered Organic Semiconductors. *J. Chem. Theory Comput.* **2011**, *7*, 3335−3345.
(17) Bassler, H.; Köhler, A. Charge Transport in Organic Semiconductors. *Top. Curr. Chem.* **2011**, *312*, 1−65.
(18) Cheung, D. L.; McMahon, D. P.; Troisi, A. A Realistic Description of the Charge Carrier Wave Function in Microcrystalline Polymer Semiconductors. *J. Am. Chem. Soc.* **2009**, *131*, 11179−11186.
(19) McMahon, D. P.; Troisi, A. An ad hoc Tight Binding Method To Study the Electronic Structure of Semiconducting Polymers. *Chem. Phys. Lett.* **2009**, *480*, 210−214.
(20) García, G.; Timón, V.; Hernández-Laguna, A.; Navarro, A.; Fernández-Gómez, M. Influence of the Alkyl and Alkoxy Side Chains on the Electronic Structure and Charge-Transport Properties of Polythiophene Derivatives. *Phys. Chem. Chem. Phys.* **2011**, *13*, 10091−10099.
(21) Bhatta, R. S.; Tsige, M. Chain Length and Torsional Dependence of Exciton Binding Energies in P3HT and PTB7 Conjugated Polymers: A First-Principles Study. *Polymer* **2014**, *55*, 2667−2672.
(22) Frost, J. M.; Kirkpatrick, J.; Kirchartz, T.; Nelson, J. Parameter Free Calculation of the Subgap Density of States in Poly(3-Hexylthiophene). *Faraday Discuss.* **2014**, *174*, 255−266.
(23) Poelking, C.; Daoulas, K.; Troisi, A.; Andrienko, D. In *P3HT Revisited — From Molecular Scale to Solar Cell Devices*; Ludwigs, S., Ed.; Advances in Polymer Science; Springer Berlin Heidelberg: Berlin, Heidelberg, 2014; Vol. *265*; pp 139−180.
(24) Gargi, D.; Kline, R. J.; DeLongchamp, D. M.; Fischer, D. A.; Toney, M. F.; O'Connor, B. T. Charge Transport in Highly Face-On Poly(3-hexylthiophene) Films. *J. Phys. Chem. C* **2013**, *117*, 17421−17428.
(25) O'Connor, B.; Kline, R. J.; Conrad, B. R.; Richter, L. J.; Gundlach, D.; Toney, M. F.; DeLongchamp, D. M. Anisotropic Structure and Charge Transport in Highly Strain-Aligned Regioregular Poly(3-hexylthiophene). *Adv. Funct. Mater.* **2011**, *21*, 3697−3705.
(26) O'Connor, B. T.; Reid, O. G.; Zhang, X.; Kline, R. J.; Richter, L. J.; Gundlach, D. J.; DeLongchamp, D. M.; Toney, M. F.; Kopidakis, N.; Rumbles, G. Morphological Origin of Charge Transport Anisotropy in Aligned Polythiophene Thin Films. *Adv. Funct. Mater.* **2014**, *24*, 3422−3431.
(27) Lücke, A.; Schmidt, W. G.; Rauls, E.; Ortmann, F.; Gerstmann, U. Influence of Structural Defects and Oxidation onto Hole Conductivity in P3HT. *J. Phys. Chem. B* **2015**, *119*, 6481−6491.
(28) Schafferhans, J.; Baumann, A.; Wagenpfahl, A.; Deibel, C.; Dyakonov, V. Oxygen Doping of P3HT:PCBM Blends: Influence on Trap States, Charge Carrier Mobility and Solar Cell Performance. *Org. Electron.* **2010**, *11*, 1693−1700.
(29) Manceau, M.; Rivaton, A.; Gardette, J.-L.; Guillerez, S.; Lemaître, N. The Mechanism of Photo- and Thermooxidation of Poly(3-Hexylthiophene) (P3HT) Reconsidered. *Polym. Degrad. Stab.* **2009**, *94*, 898−907.
(30) Sperlich, A.; Kraus, H.; Deibel, C.; Blok, H.; Schmidt, J.; Dyakonov, V. Reversible and Irreversible Interactions of Poly(3-Hexylthiophene) with Oxygen Studied by Spin-Sensitive Methods. *J. Phys. Chem. B* **2011**, *115*, 13513−13518.
(31) Grossiord, N.; Kroon, J. M.; Andriessen, R.; Blom, P. W. M. Degradation Mechanisms in Organic Photovoltaic Devices. *Org. Electron.* **2012**, *13*, 432−456.
(32) Chabinyc, M. L.; Street, R. A.; Northrup, J. E. Effects of Molecular Oxygen and Ozone on Polythiophene-Based Thin-Film Transistors. *Appl. Phys. Lett.* **2007**, *90*, 123508.
(33) Norrman, K.; Madsen, M. V.; Gevorgyan, S. A.; Krebs, F. C. Degradation Patterns in Water and Oxygen of an Inverted Polymer Solar Cell. *J. Am. Chem. Soc.* **2010**, *132*, 16883−16892.
(34) Lin, Y.-J.; Tsai, C.-L.; Su, Y.-C.; Liu, D.-S. Carrier Transport Mechanism of Poly(3,4-ethylenedioxythiophene) doped with poly(4-styrenesulfonate) Films by Incorporating ZnO Nanoparticles. *Appl. Phys. Lett.* **2012**, *100*, 253302.
(35) Bhattacharya, S.; Malik, S.; Nandi, A. K.; Ghosh, A. Transport Properties of CdS Nanowire Embedded Poly(3-hexyl thiophene) Nanocomposite. *J. Chem. Phys.* **2006**, *125*, 174717.
(36) Salleo, A. Charge Transport in Polymeric Transistors. *Mater. Today* **2007**, 38−45.
(37) Wang, C.; Jimison, L. H.; Goris, L.; McCulloch, I.; Heeney, M.; Ziegler, A.; Salleo, A. Microstructural Origin of High Mobility in High-Performance Poly(thieno-thiophene) Thin-Film Transistors. *Adv. Mater.* **2010**, 697−701.
(38) Muhammad, A. K.; Sun, J.-X. Sun Improvement of Mobility Edge Model by using New Density of States with Exponential Tail for Organic Diode. *Chin. Phys. B* **2015**, No. 047203, DOI: 10.1088/1674-1056/24/4/047203.
(39) Chang, J.-F.; Sirringhaus, H.; Giles, M.; Heeney, M.; McCulloch, I. Relative Importance of Polaron Activation and Disorder on Charge Transport in High-Mobility Conjugated Polymer Field-Effect Transistors. *Phys. Rev. B* **2007**, *76*, 205204.

DOI: 10.1021/acs.jpcb.6b03598
J. Phys. Chem. B 2016, 120, 5572−5580

(40) Kubo, R. Statistical-Mechanical Theory of Irreversible Processes. I. General Theory and Simple Applications to Magnetic and Conduction Problems. *J. Phys. Soc. Jpn.* **1957**, *12*, 570−586.
(41) Holstein, T. Studies of Polaron Motion. *Ann. Phys.* **1959**, *8*, 343−389.
(42) Ortmann, F.; Bechstedt, F.; Hannewald, K. Theory of Charge Transport in Organic Crystals: Beyond Holstein's Small-Polaron Model. *Phys. Rev. B* **2009**, *79*, 235206.
(43) Ortmann, F.; Bechstedt, F.; Hannewald, K. Charge Transport in Organic Crystals: Interplay of Band Transport, Hopping and Electron-Phonon Scattering. *New J. Phys.* **2010**, *12*, No. 023011, DOI: 10.1088/1367-2630/12/2/023011.
(44) Ortmann, F.; Bechstedt, F.; Hannewald, K. Charge Transport in Organic Crystals: Theory and Modelling. *Phys. Status Solidi B* **2011**, *248*, 511−525.
(45) Motta, C.; Sanvito, S. *J. Chem. Theory Comput.* **2014**, *10*, 4624.
(46) Ortmann, F.; Hannewald, K.; Bechstedt, F. Charge Transport in Guanine-Based Materials. *J. Phys. Chem. B* **2009**, *113*, 7367−7371.
(47) Kresse, G.; Furthmüller, J. Efficiency of Ab-initio Total Energy Calculations for Metals and Semiconductors using a Plane-Wave Basis Set. *Comput. Mater. Sci.* **1996**, *6*, 15.
(48) Blöchl, P. E. Projector Augmented-Wave Method. *Phys. Rev. B* **1994**, *50*, 17953−17979.
(49) Perdew, J.; Burke, K.; Ernzerhof, M. Generalized Gradient Approximation Made Simple. *Phys. Rev. Lett.* **1996**, *77*, 3865−3868.
(50) Perdew, J.; Burke, K.; Ernzerhof, M. Generalized Gradient Approximation Made Simple [Phys. Rev. Lett. 77, 3865 (1996)]. *Phys. Rev. Lett.* **1997**, *78*, 1396.
(51) Colle, R.; Grosso, G.; Ronzani, A.; Zicovich-Wilson, C. M. Structure and X-ray Spectrum of Crystalline Poly(3-Hexylthiophene) from DFT-van der Waals Calculations. *Phys. Status Solidi B* **2011**, *248*, 1360−1368.
(52) London, F. *Z. Phys. Chem., Abt. B* **1930**, 222.
(53) Yoshizawa, K.; Yumura, T.; Yamabe, T.; Bandow, S. The Role of Orbital Interactions in Determining the Interlayer Spacing in Graphite Slabs. *J. Am. Chem. Soc.* **2000**, *122*, 11871−11875.
(54) Ortmann, F.; Schmidt, W. G.; Bechstedt, F. Attracted by Long-Range Electron Correlation: Adenine on Graphite. *Phys. Rev. Lett.* **2005**, *95*, 186101.
(55) Grimme, S. Semiempirical GGA-Type Density Functional Constructed with a Long-Range Dispersion Correction. *J. Comput. Chem.* **2006**, *27*, 1787−1799.
(56) Monkhorst, H. J.; Pack, J. D. Special Points for Brillouin-Zone Integrations. *Phys. Rev. B* **1976**, *13*, 5188−5192.
(57) Horovitz, B.; Österbacka, R.; Vardeny, Z. V. Multiple Fano Effect in Charge Density Wave Systems. *Synth. Met.* **2004**, *141*, 179−183.
(58) Österbacka, R.; Jiang, X. M.; An, C. P.; Horovitz, B.; Vardeny, Z. V. Photoinduced Quantum Interference Antiresonances in π-Conjugated Polymers. *Phys. Rev. Lett.* **2002**, *88*, 88.
(59) Hannewald, K. Theory of Polaron Bandwidth Narrowing in Organic Molecular Crystals. *Phys. Rev. B* **2004**, *69*, No. 075211.
(60) The experimental fit parameters contain a prominent mode at about 250 meV which matches neither the experimental frequencies nor the present calculations which predict a phonon gap between 190 and 363 meV, in agreement with Raman and Fourier transform infrared spectroscopy (FTIR) in ref 76.
(61) Salleo, A.; Chen, T. W.; Völkel, A. R.; Wu, Y.; Liu, P.; Ong, B. S.; Street, R. A. Intrinsic Hole Mobility and Trapping in a Regioregular Poly(thiophene). *Phys. Rev. B* **2004**, 70.
(62) Street, R. A.; Northrup, J. E.; Salleo, A. Transport in Polycrystalline Polymer Thin-Film Transistors. *Phys. Rev. B* **2005**, 71.
(63) Zen, A.; Pflaum, J.; Hirschmann, S.; Zhuang, W.; Jaiser, F.; Asawapirom, U.; Rabe, J. P.; Scherf, U.; Neher, D. Effect of Molecular Weight and Annealing of Poly(3-hexylthiophene)s on the Performance of Organic Field-Effect Transistors. *Adv. Funct. Mater.* **2004**, *14*, 757−764.
(64) Chang, J.-F.; Clark, J.; Zhao, N.; Sirringhaus, H.; Breiby, D.; Andreasen, J.; Nielsen, M.; Giles, M.; Heeney, M.; McCulloch, I. Molecular-Weight Dependence of Interchain Polaron Delocalization and Exciton Bandwidth in High-Mobility Conjugated Polymers. *Phys. Rev. B* **2006**, *74*, 115318.
(65) Scharsich, C.; Lohwasser, R. H.; Sommer, M.; Asawapirom, U.; Scherf, U.; Thelakkat, M.; Neher, D.; Köhler, A. Control of Aggregate Formation in Poly(3-hexylthiophene) by Solvent, Molecular Weight, and Synthetic Method. *J. Polym. Sci., Part B: Polym. Phys.* **2012**, *50*, 442−453.
(66) Northrup, J. Atomic and Electronic Structure of Polymer Organic Semiconductors: P3HT, PQT, and PBTTT. *Phys. Rev. B* **2007**, *76*, 245202.
(67) Farchioni, R.; Grosso, G., Ed. *Organic Electronic Materials*; Springer, 2001; Vol. *41*.
(68) Kelley, T. W.; Frisbie, C. D. Gate Voltage Dependent Resistance of a Single Organic Semiconductor Grain Boundary. *J. Phys. Chem. B* **2001**, *105*, 4538−4540.
(69) Chwang, A. B.; Frisbie, C. D. Temperature and Gate Voltage Dependent Transport Across a Single Organic Semiconductor Grain Boundary. *J. Appl. Phys.* **2001**, *90*, 1342.
(70) Jimison, L. H.; Toney, M. F.; McCulloch, I.; Heeney, M.; Salleo, A. Charge-Transport Anisotropy Due to Grain Boundaries in Directionally Crystallized Thin Films of Regioregular Poly(3-hexylthiophene). *Adv. Mater.* **2009**, *21*, 1568−1572.
(71) Kline, R. J.; McGehee, M. D.; Kadnikova, E. N.; Liu, J.; Fréchet, J. M. J.; Toney, M. F. Dependence of Regioregular Poly(3-hexylthiophene) Film Morphology and Field-Effect Mobility on Molecular Weight. *Macromolecules* **2005**, *38*, 3312−3319.
(72) Liu, C.; Oshima, K.; Shimomura, M.; Miyauchi, S. Anisotropic Conductivity—Temperature Characteristic of Solution-Cast Poly(3-hexylthiophene) Films. *Synth. Met.* **2006**, *156*, 1362−1367.
(73) Joshi, S.; Pingel, P.; Grigorian, S.; Panzner, T.; Pietsch, U.; Neher, D.; Forster, M.; Scherf, U. Bimodal Temperature Behavior of Structure and Mobility in High Molecular Weight P3HT Thin Films. *Macromolecules* **2009**, *42*, 4651−4660.
(74) Ortmann, F.; Radke, K. S.; Günther, A.; Kasemann, D.; Leo, K.; Cuniberti, G. Materials Meets Concepts in Molecule-Based Electronics. *Adv. Funct. Mater.* **2015**, *25*, 1933−1954.
(75) Brown, P. J.; Thomas, D. S.; Köhler, A.; Wilson, J. S.; Kim, J.-S.; Ramsdale, C. M.; Sirringhaus, H.; Friend, R. H. Effect of Interchain Interactions on the Absorption and Emission of Poly(3-hexylthiophene). *Phys. Rev. B* **2003**, *67*, 064203.
(76) Louarn, G.; Trznadel, M.; Buisson, J. P.; Laska, J.; Pron, A.; Lapkowski, M.; Lefrant, S. Raman Spectroscopic Studies of Regioregular Poly(3-alkylthiophenes). *J. Phys. Chem.* **1996**, *100*, 12532−12539.
(77) Humphrey, W.; Dalke, A.; Schulten, K. VMD: Visual Molecular Dynamics. *J. Mol. Graphics* **1996**, *14*, 33−38.

DOI: 10.1021/acs.jpcb.6b03598
J. Phys. Chem. B 2016, 120, 5572−5580